

1 **BrGDGTs-based seasonal paleotemperature reconstruction for the last 15,000 years from**
2 **a shallow lake on the eastern Tibetan Plateau**

3 Xiaohuan Hou ^a, Nannan Wang ^a, Zhe Sun ^b, Kan Yuan ^{a, c}, Xianyong Cao ^a, Juzhi Hou ^{a *}

4 ^a *Group of Alpine Paleoecology and Human Adaptation (ALPHA), State Key Laboratory of Tibetan*
5 *Plateau Earth System, Resources and Environment (TPESRE), Institute of Tibetan Plateau Research,*
6 *Chinese Academy of Sciences, Beijing 100101, China*

7 ^b *Institute of Geography and Resources Science, Sichuan Normal University, Chengdu, 610066, China*

8 ^c *University of Chinese Academy of Sciences, Beijing 100049, China*

9

10 * Corresponding author

11 E-mail address: houjz@itpcas.ac.cn

12

13 **ABSTRACT**

14 Understanding Holocene temperature changes is vital for resolving discrepancies between
15 proxy reconstructions and climate models. The intricate temperature variations across the
16 Tibetan Plateau (TP) add complexity to studying continental climate change during this
17 period. Discrepancies between model-based and proxy-based reconstructions might stem
18 from seasonal biases and environmental uncertainties in the proxies. Employing multiple
19 proxies from a single sediment core for quantitative temperature reconstructions offers an
20 effective method for cross-validation in terrestrial environments. Here, we present an ice-
21 free-season temperature record for the past 15 ka from a shallow, freshwater lake on the
22 eastern TP, based on brGDGTs (branched glycerol dialkyl glycerol tetraethers). This record
23 shows that the Holocene Thermal Maximum lags the pollen-based July temperature recorded
24 in the same sediment core. We conclude that the mismatch between the brGDGTs-based and
25 pollen-based temperatures is primarily the result of seasonal variations in solar irradiance.
26 The overall pattern of temperature changes is supported by other summer temperature
27 records, and the Younger Dryas cold event and the Bølling–Allerød warm period are also
28 detected. A generally warm period occurred during 8–3.5 ka, followed by a cooling trend in
29 the late Holocene. Our findings have implications for understanding the seasonal signal of
30 brGDGTs in shallow lakes, and provide critical data for confirming the occurrence of
31 seasonal biases in different proxies from high-elevation lakes. To further investigate the
32 significance of the brGDGTs and temperature patterns on the TP, we examined existing
33 brGDGTs-based Holocene temperature records, which interpret these compounds as
34 indicators of mean annual or growing season temperatures. The existing/available

35 temperature records show complicated patterns of variation, some with general warming
36 trends throughout the Holocene, some with cooling trends, while some with warm middle
37 Holocene. We analyzed the possible reasons for the diverse brGDGTs records on the TP and
38 emphasize the importance of considering lake conditions and modern investigations of
39 brGDGTs in lacustrine systems when using brGDGTs to reconstruct paleoenvironmental
40 conditions.

41 **Keywords:** Tibetan Plateau, brGDGTs, the mean temperature of Months Above Freezing,
42 shallow lake, Holocene

43 **1 Introduction**

44 Global climate change has a profound impact on both the natural ecological and socio-
45 economic systems that are vital for human survival and development, making climate change
46 a critical limiting factor for the sustainable development of human society. The Tibetan Plateau
47 (TP), also called the “Third Pole” (Qiu, 2008), has undergone a more rapid warming over the
48 last five decades, with a rate twice that of the global average ($0.3 - 0.4^{\circ}\text{C}/\text{decade}$) (Kuang and
49 Jiao, 2016; Chen et al., 2015), making it one of the world's most temperature-sensitive regions
50 (Chen et al., 2015; Yao et al., 2022). Consequently, assessing the impact of future climate
51 change on the TP is becoming increasingly important. To enhance the precision and accuracy
52 of future climate change estimates for the TP under ongoing global climate change and to
53 minimize the uncertainty in climate simulations, it is essential to investigate the processes and
54 mechanisms of regional climate and environmental changes, with particular emphasis on
55 temperature, on a relatively long timescale, such as that of the Holocene.

56

57 The Holocene, the most recent geological epoch, is closely linked with the development of
58 human civilization. Quantitative reconstructions of Holocene temperature trends can be used
59 to explore their impacts on civilization and to establish a geological and historical context for
60 predicting future climate changes. In recent decades, many Holocene quantitative
61 reconstructions of seasonal and annual temperatures for the TP have been produced using
62 various proxies, like pollen (Herzschuh et al., 2014; Lu et al., 2011), chironomids (Zhang et al.,
63 2017; Zhang et al., 2019a), $\delta^{18}\text{O}$ in ice cores (Pang et al., 2020; Thompson et al., 1997), and
64 biomarkers (Hou et al., 2016; Zhao et al., 2013; Cheung et al., 2017). These reconstructions
65 have provided crucial data for the elucidation of Holocene temperature changes. However, the
66 available Holocene temperature records from the TP show divergent trends. Multiple proxy
67 indicators indicate three different Holocene temperature patterns on the TP. First, a consistent
68 Holocene warming trend (Sun et al., 2022; Feng et al., 2022; Opitz et al., 2015). For example,
69 brGDGTs based annual temperatures (Feng et al., 2022; Sun et al., 2022) indicate a gradual
70 warming trend which resembles the $\delta^{18}\text{O}$ temperature record from the Chongce ice core on the
71 western TP, except for the last 2 ka (Pang et al., 2020). Second, an early to middle Holocene
72 summer temperature maximum and a gradual cooling trend during the late Holocene are
73 observed in pollen-, alkenone- and chironomid-based temperature records (Herzschuh et al.,
74 2014; Hou et al., 2016; Zhang et al., 2017; Wang et al., 2021a; Zheng et al., 2015). Third, a
75 prominent relatively cool middle Holocene (Wang et al., 2021c; Li et al., 2017); for example,
76 a composite temperature record suggests that temperatures were $\sim 2^\circ\text{C}$ cooler during the middle
77 Holocene than during the early and late Holocene (Wang et al., 2021c). Several records also
78 show a steady long-term trend without distinct cooling or warming (Sun et al., 2021). Moreover,

79 the cooling trends in proxy-based Holocene temperature records are inconsistent with those of
80 climate models, which indicate a warming trend, and this inconsistency is widely known as the
81 “Holocene temperature conundrum” (Liu et al., 2014). There are several potential factors that
82 may contribute to the disparity in Holocene temperature trends, including seasonal biases and
83 uncertainties in temperature proxies and reconstructions, independent of climate models (Liu
84 et al., 2014; Hou et al., 2019; Bova et al., 2021; Cartapanis et al., 2022; Marsicek et al., 2018).
85 While several recent studies have suggested that seasonality in proxies is not the major cause
86 of the Holocene temperature conundrum (Dong et al., 2022; Zhang et al., 2022b), it is
87 significant that the TP is an alpine and high-altitude region with significant seasonal
88 temperature variations. Moreover, most organisms tend to grow during the warmer seasons at
89 high latitudes and high altitudes (Zhao et al., 2021a). Currently, however, we lack unambiguous
90 and reliable seasonal temperature records to support a seasonality-bias hypothesis. Extensive
91 research has been conducted in lakes, employing a single proxy to reconstruct past temperature
92 fluctuations. However, there have been scarce studies that employ various proxies within the
93 same core to reconstruct paleotemperature variations. Furthermore, the limited number of
94 studies primarily concentrate on reconstructing summer temperature and annual average
95 temperature. For example, a chironomid-based July temperature reconstruction for Tiancai lake
96 on the southeastern TP shows higher temperatures during the early to middle Holocene (Zhang
97 et al., 2017), while the brGDGTs-based annual average temperature shows a warming trend
98 (Feng et al., 2022). Different proxies may reflect the seasonal temperatures in different months,
99 and thus producing temperature reconstructions for different months for the same sediment
100 core may help better understand the seasonal bias of terrestrial temperature records.

101 Furthermore, the reconciliation of the divergent trends of Holocene temperature on the TP and
102 its surroundings requires additional high-altitude temperature records from these regions, with
103 reliable chronologies and proxy records with an unambiguous climatological significance.

104

105 Branched glycerol dialkyl glycerol tetraethers (brGDGTs) are a group of membrane-spanning
106 lipids found in bacteria (Fig. S1) (Chen et al., 2022; Halamka et al., 2022; Sinninghe Damsté
107 et al., 2000), and they have become a powerful tool for quantifying past terrestrial temperature
108 variations. Through investigations of brGDGTs in globally-distributed soils, it was found that
109 the distribution of brGDGTs is primarily related to temperature and pH (Weijers et al., 2007).
110 Subsequently, brGDGTs–temperature calibrations from soil, peat and lake sediments were
111 established on scales from global (Weijers et al., 2007; De Jonge et al., 2014; Crampton-Flood
112 et al., 2020; Martínez-Sosa et al., 2021) to regional (e.g., East Asia) (Sun et al., 2011; Ding et
113 al., 2015; Wang et al., 2016; Dang et al., 2018), leading to considerable progress in
114 reconstructing terrestrial temperatures, particularly on the TP (Cheung et al., 2017; Zhang et
115 al., 2022a; Li et al., 2017).

116

117 Natural lakes are widely distributed across the TP (Zhang et al., 2019b). Lake sediments,
118 characterized by their organic matter-rich composition, exhibit continuous and rapid
119 accumulation rates. As a result, they offer high-resolution records of environmental changes,
120 making them highly valued as a primary terrestrial climate archive (Moser et al., 2019).
121 BrGDGTs in lacustrine systems are often more strongly correlated with temperature, with
122 higher coefficient of determination (r^2) and lower root mean square error (RMSE) values

123 (Martínez-Sosa et al., 2021), than in soils and peats. Nevertheless, the factors that impact the
124 distribution of brGDGTs in lakes are intricate and multidimensional. Notably, the sources of
125 brGDGTs within lakes are intricate, involving contributions from soil as well as autochthonous
126 lake processes. However, an expanding body of research underscores a substantial prevalence
127 of autochthonous brGDGTs in lakes (Tierney and Russell, 2009; Tierney et al., 2010; Weber et
128 al., 2015; Wang et al., 2021b). Furthermore, the origins of brGDGT producers remain uncertain
129 and could be influenced by various factors, including lake salinity (Wang et al., 2021b), redox
130 conditions (Weber et al., 2018), oxygen content and/or mixing patterns (Van Bree et al., 2020;
131 Wu et al., 2021; Buckles et al., 2014). Additionally, even lake depth plays a role due to distinct
132 ecological niches (Woltering et al., 2012), thereby contributing to the intricate interplay that
133 shapes the distribution of brGDGTs within lakes.

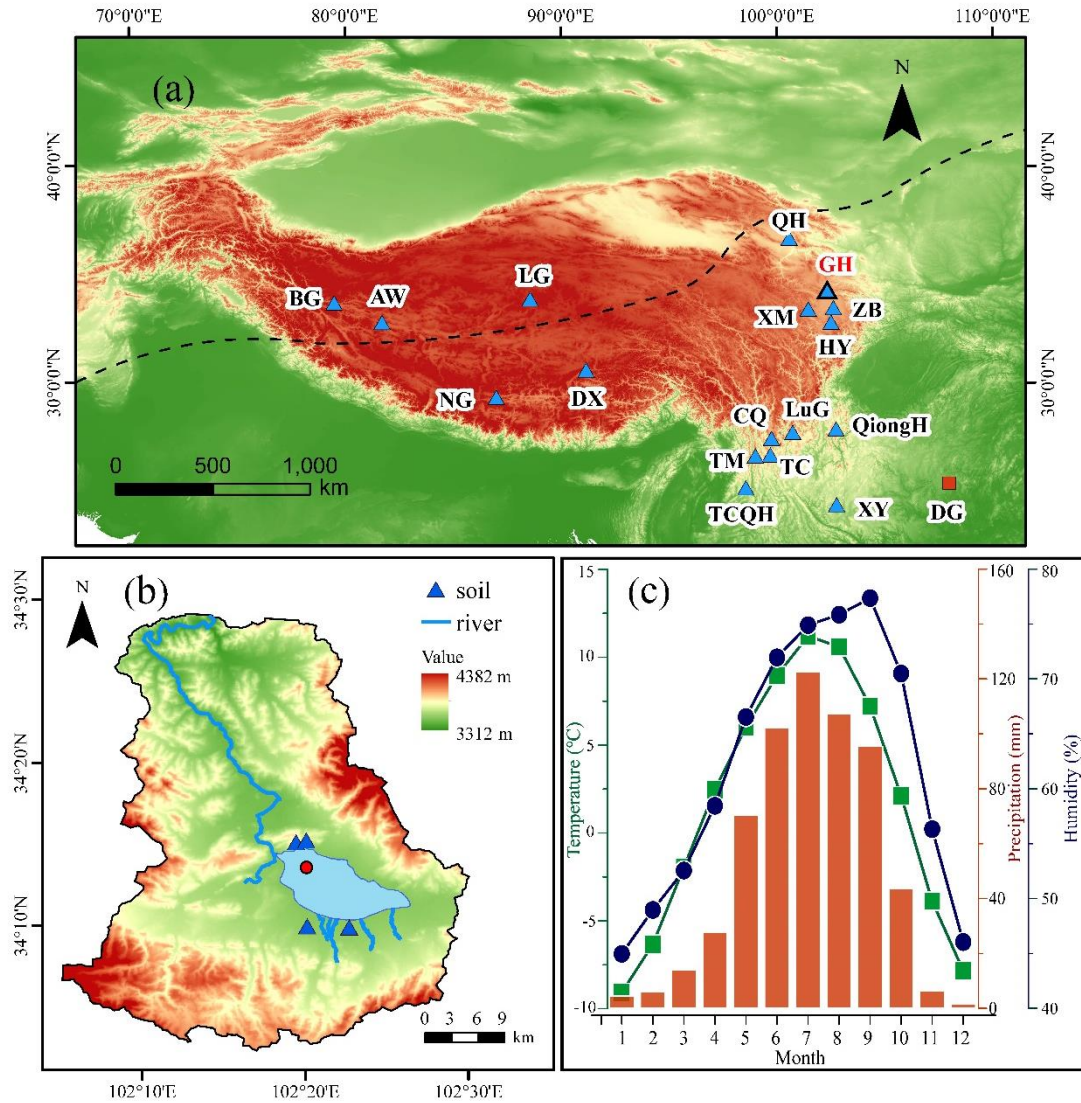
134

135 In this study, we obtained a quantitative temperature reconstruction for the past 15 ka from
136 Gahai, a shallow (average depth of ~2 m) freshwater lake located in the source area of the
137 Yellow River. This region is an important ecological protection area on the eastern edge of the
138 TP. Freshwater environments avoid the confounding effects of salinity on brGDGTs-based
139 temperature reconstructions, and shallow lakes also minimize the impact of the uneven
140 distribution of light and nutrients on brGDGTs. Our specific aims were: (1) to determine the
141 long-term trend of Holocene warm-biased terrestrial temperatures at a high elevation; (2) to
142 compare records of ice-free season temperatures with July temperatures from the same
143 sediment core; and (3) to gain a better understanding of the possible mechanisms responsible
144 for Holocene temperature variations, especially on the TP.

145 **2 Materials and methods**

146 *2.1 Study site*

147 Gahai (102°11'–102°28' E, 34°04'–34°4' N, 3444 m a.s.l.) is a freshwater lake and part of the
148 Gahai meadow wetland, which is a national nature reserve with restricted human access, on the
149 eastern edge of the TP (Fig. 1). The lake is fed by runoff from the surrounding hills, drains into
150 the Tao River, and ultimately enters the Yellow River. Thus, Gahai lake is a critical water
151 conservation area in the upper reaches of the Yellow River. The average water depth of Gahai
152 is ~2 m, and the maximum depth is ~5 m. The vegetation in the catchment consists mainly of
153 *Kobresia tibetica*, *Equisetum arvense*, *Potentilla anserina*, *Artemisia subulate*, and *Oxytropis*
154 *falcata* (Ma et al., 2019). Meteorological data for the area are available from Langmu Temple
155 station (1957-1988) (Fig. 1) (102°38' E, 34°5' N, 3412 m a.s.l.), ~32 km northwest of Gahai
156 lake. They indicate an annual average (mean) precipitation of 781 mm, with > 67% occurring
157 between June and September, and mean annual temperature of 1.2 °C with a relative humidity
158 of ~65%. The summers are mild and humid and the winters are cold and dry. From May to
159 September, the mean average temperature is above freezing (0°C), but the temperature in May
160 is very low, close to 0°C.



161

162

163

164

165

166

167

168

169

170

171

172

Fig. 1 (a) Locations of the sites on the Tibetan Plateau referenced in the text. Triangle with bold line indicates the location of Gahai lake (this study). Other triangles indicate the locations of cited studies on the TP and the surrounding area: Bangong Co (BG), Aweng Co (AW), Ngamring Co (NG), Linggo Co (LG), Dangxiong wetland (DX), Qinghai lake (QH), Ximen Co (XM), Zoige Basin (ZB), Hongyuan peatland (HY), Lugu lake (LuG), Cuoqia lake (CQ), Tingming lake (TM), Tengchongqinghai lake (TCQH), Tiancai lake (TC), Qionghai lake (QH), Xingyun lake (XY). Red square indicates Dongge Cave (DG). Black dotted line represents the northern boundary of the modern Asian summer Monsoon (Chen et al., 2008). (b) Drainage basin of Gahai lake and the core site. (c) Climate data from Langmu Temple meteorological station: monthly temperature (green line), precipitation (red bars), and humidity (navy blue line).

173 *2.2 Sampling*

174 A sediment core with the length of 329 cm was obtained from Gahai lake in January 2019, at
175 a water depth of 1.95 m, using a UWITEC platform operated from the frozen lake surface. In
176 addition, four catchment soil samples were collected from around the lake (Fig. 1). All samples
177 were transported to the Institute of Tibetan Plateau Research, Chinese Academy of Sciences
178 (ITPCAS). The sediment core was split lengthwise, and one half was subsampled and freeze-
179 dried for subsequent analysis.

180

181 *2.3 Chronology*

182 The chronology of the upper 20 cm of the sediment core is based on measurements of ^{210}Pb
183 and ^{137}Cs , at a 1-cm interval. The chronology for the deeper part of the core is provided by
184 accelerator mass spectrometry (AMS) ^{14}C measurements of 13 bulk sediment samples, which
185 were conducted by Beta Analytic Inc. (Miami, USA) (Fig. 2) (Wang et al., 2022).

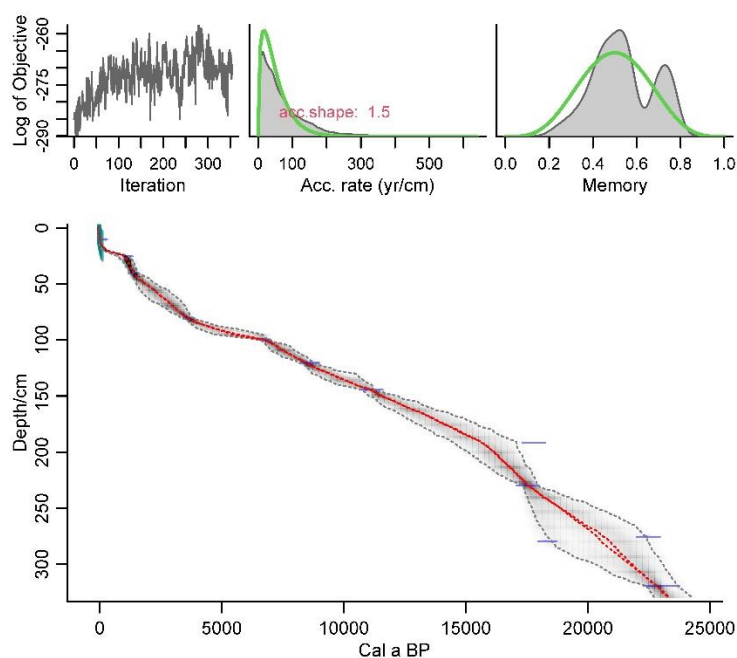
186

187 The ^{210}Pb age model was constructed using the constant rate of supply (CRS) model and the
188 ^{137}Cs peak was used as supplement (Appleby, 2002). The calculated age of ^{210}Pb using CRS
189 model aligned well with the ^{137}Cs peak at 6 cm. Overall, the CRS model was deemed suitable
190 for determining the age of Gahai lake.

191

192 Reservoir age, as highlighted by Hou et al. (2012), is a crucial factor affecting the age
193 determination of lake sediment cores on the TP. Therefore, it was necessary to establish the
194 reservoir age of Gahai lake before undertaking paleoclimate reconstruction. The linear

195 extrapolation relationship between the ^{14}C ages and depth to the sediment-water interface is
196 often used to estimate the reservoir age. The ^{14}C age of 13 samples exhibits a good linear
197 relationship with sediments depth in Gahai lake. Extrapolation of this 13 ^{14}C ages down to the
198 depth of 6 cm yielded a ^{14}C age of 461 yr BP, while the reliable ^{210}Pb age at 6 cm is -27 yr BP.
199 Consequently, the difference between the two ages, which amounts to 488 yr, was taken as the
200 reservoir age. Additionally, it's worth noting that independent estimations of the ^{14}C calibration
201 age and ^{210}Pb age around 10 cm in Gahai lake was obtained, resulting in values of 497 yr BP
202 and 18 yr BP, respectively. The difference of 479 yr between these two ages can also be
203 considered as the reservoir age. These two methods of estimating reservoir age of Gahai lake
204 show very close, which are mutually supportive. So, the average of 483 yr was adopted as the
205 reservoir age. All original ^{14}C dates were corrected by subtracting the reservoir age (483 yr)
206 and calibrating them to calendar ages using Calib 8.1. The age-depth model (Fig. 2) was
207 constructed using the Bacon program with the ^{14}C ages and ^{210}Pb ages (Blaauw and Andres
208 Christen, 2011) and was reported by Wang et al. (2022).



209

210 **Fig. 2** Age-depth model for Gahai, based on AMS ^{14}C , ^{210}Pb and ^{137}Cs ages (Wang et al.,
211 2022). The ages of the upper 20 cm are based on ^{210}Pb and ^{137}Cs dating (green symbols)
212 and those of the lower part on AMS ^{14}C dates (blue symbols).

213

214 *2.4 Lipids extraction and brGDGTs analysis*

215 For lipids extraction, ~5 g samples were ground to a powder and extracted ultrasonically with
216 dichloromethane (DCM): methanol (MeOH) (9: 1, v: v) three times. The supernatants were
217 combined and dried under a stream of nitrogen gas. Subsequently, the total lipid extracts were
218 separated into neutral and acid fractions through a LC-NH₂ silica gel column using DCM:
219 isopropyl alcohol (2: 1, v: v) and ether with 4% acetic acid (v: v), respectively. The neutral
220 fraction was then eluted through a silica gel column using *n*-Hexane, DCM and MeOH, and
221 the GDGTs were dissolved in the MeOH. The GDGTs fraction was passed through a 0.45 μm
222 polytetrafluoroethylene (PTFE) filter before analysis. C₄₆-GDGT (a standard compound)
223 (Huguet et al., 2006) was added to the samples before analysis.

224

225 BrGDGTs were detected using an HPLC-APCI-MS (Waters ACQUITY UPLC I-Class/Xevo
226 TQD) with auto-injection at the ITPCAS. The compounds were separated by three Hypersil
227 Gold Silica LC columns in sequence (each 100 mm \times 2.1 mm, 1.9 μm , Thermo Fisher Scientific;
228 USA), maintained at a temperature of 40°C. GDGTs were eluted isocratically using 84%
229 hexane and 16% ethyl acetate (EtOA) for the first 5 min, followed by a linear gradient change
230 to 82% hexane and 18% EtOA from 5 to 65 min. The columns were cleaned using 100% EtOA
231 for 10 min, and then back to 84% hexane and 16% EtOA to equilibrate the column, with a flow
232 rate of 0.2 ml min⁻¹.

233

234 The APCI-MS conditions were as follows: nebulizer pressure at 60 psi, APCI probe
235 temperature at 400°C, drying gas flow rate of 6 L/min and temperature of 200°C, capillary
236 voltage of 3600 V, source corona of 5.5 μ A. Detection was performed in selected ion
237 monitoring (SIM) mode, targeting the protonated molecules at m/z 1050, 1048, 1046, 1036,
238 1034, 1032, 1022, 1020, 1018 and 744. The results were analyzed using MassLynx V4.1
239 software, and quantification was achieved by comparing the peak areas of targeted ions and the
240 internal standard, assuming an identical response factor for GDGTs.

241

242 **3 Results and Discussion**

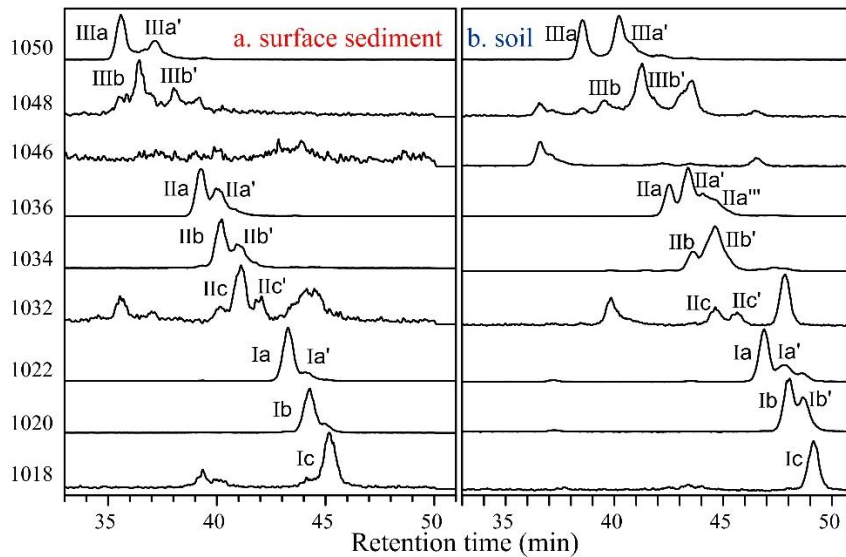
243 *3.1. Concentration and distribution of brGDGTs in the sediment core and catchment soils*

244 BrGDGTs were detected in both the catchment soils and the downcore sediments. The average
245 concentration of brGDGTs in the catchment soils (0.07 ng g⁻¹dw) was lower than in the surficial
246 core sediments (0.70 ng g⁻¹dw). In the soil samples, pentamethylated brGDGTs were generally
247 the most abundant (55.33%), followed by tetramethylated brGDGTs (23.60%) and
248 hexamethylated brGDGTs (21.07%) (Fig. S2). The relative amount of cyclopentane ring-
249 containing brGDGTs in the soil samples was generally low (24.34%) and it was sometimes too
250 low to be detected, especially the fractions of IIIb, IIIb', IIIc, IIIc', IIc and IIc'. In the downcore
251 sediments, the relative abundant of tetramethylated brGDGTs (43.84%) was like that of
252 pentamethylated brGDGTs (41.93%), and hexamethylated brGDGTs were the least abundant
253 (14.22%) (Fig. S2). The relative abundant of cyclopentane ring-containing brGDGTs in the
254 downcore sediments (67.82%) was lower than that in the catchment soils.

255 3.2 *In situ* production of brGDGTs in Gahai lake

256 Although lacustrine brGDGTs have great potential for quantitatively reconstructing terrestrial
257 paleotemperatures, uncertainties about their sources in lacustrine environments are a major
258 factor limiting their application (Tierney and Russell, 2009; Cao et al., 2020; Sun et al., 2011;
259 Sinninghe Damsté et al., 2009; Buckles et al., 2014). To investigate the origin and
260 characteristics of brGDGTs in Gahai lake sediments, we examined the distributions and
261 concentrations of brGDGTs in the sediments and catchment soils and found notable differences
262 between them. First, as described in the previous section, the average content of brGDGTs in
263 the catchment soils was ~10% that of the surficial lake sediments, suggesting the absence of
264 large-scale allochthonous inputs from the catchment soils. Second, the brGDGTs distributions
265 in the downcore sediments were quite different from those in the catchment soils, which
266 suggests a substantial autochthonous brGDGTs contribution to the lake sediments (Fig. 3 and
267 Fig. S2). Moreover, the ratios of 6-methyl brGDGTs to 5-methyl GDGTs (IR_{6ME}) in the soils
268 and sediments, calculated according to the formula proposed by De Jonge et al. (2014), were
269 different. In the soil samples, IR_{6ME} varied between 0.54 and 0.57 and the average ratio in the
270 downcore samples was 0.26, varying between 0.18 and 0.47. Third, the in-situ production of
271 brGDGTs in Gahai lake is suggested by the discrepancies in the degree of methylation
272 (MBT'_{5ME}) between the soils and surface sediments. The average value of MBT'_{5ME} in the
273 Gahai lake surface sediments was 0.48, which is clearly higher than in the catchment soils,
274 with the range of 0.32–0.35. Fourth, and potentially the most significant, the IIIb' and Ib'
275 compounds are present in the catchments soil but not in the Gahai lake surficial sediments,
276 which may be direct evidence of an autochthonous brGDGTs contribution in the lacustrine

277 environment (Fig. 3), and a lower proportion of soil-derived brGDGTs input. Therefore, we
278 conclude that the brGDGTs in the Gahai lake sediments are mainly of in-situ origin.



279

280 **Fig. 3** Representative high-performance liquid chromatography/atmospheric pressure
281 chemical ionization-mass spectrometry (HPLC/APCIMS) chromatograms of brGDGTs
282 from (a) surface sediments from Gahai lake, and (b) soils in the catchment of Gahai
283 lake.

284

285 3.3 brGDGTs-temperature calibration and Holocene temperature reconstruction

286 Gahai is a shallow lake in the eastern TP that is typically completely frozen during winter and
287 spring. Local meteorological data indicate that the average snowfall period lasts for 269 days,
288 with around 50 days of continuous snowfall (Liang and Luo, 2006). The freezing of the lake
289 surface begins in late October each year and gradually thaws starting from May of the following
290 year. As a result, the light transmittance and oxygen content in the lake water are reduced during
291 the freezing season, leading to decreased nutrient levels, which severely hinder the growth of
292 autotrophic microorganisms. Although the bacteria responsible for producing brGDGTs have

293 not been thoroughly characterized, the abundance of heterotrophic bacteria will likely decrease
294 due to the reduced autotrophic biomass during the winter and spring ice-covered period. The
295 weakened light penetration, decreased oxygen levels, and lack of nutrient replenishment during
296 the frozen period significantly impact the growth of autochthonous microorganisms.

297

298 Furthermore, some research suggests that the production of brGDGTs might be related to
299 factors such as water depth, seasonal alternation of water column mixing and stratification
300 (Loomis et al., 2014; Van Bree et al., 2020). During the summer and autumn seasons when the
301 lake ice melts and the water becomes more mobile, the nutrient content increases, resulting in
302 elevated lake biomass, moreover, the oxygen levels at the bottom of Gahai lake are not expected
303 to be too high, which could further contribute to the proliferation of brGDGT-producing
304 bacteria, potentially leading to an increase in the brGDGT-producing bacteria (Weber et al.,
305 2018). Therefore, brGDGTs in Gahai lake may provide records of the average temperature
306 during the ice-free months of the summer and autumn seasons.

307

308 Additionally, the presence of the frozen lake surface during winter creates a thermal barrier,
309 impeding the exchange of heat between the lake water and the atmosphere. Consequently, any
310 brGDGTs generated within the lake water during this period lose their ability to accurately
311 reflect atmospheric temperature variations (Sun et al., 2021; Zhang et al., 2022a). Thus, they
312 were no longer able to track atmospheric temperature changes during the frozen season. So, we
313 prefer to use Gahai brGDGTs to reconstruct temperatures during the summer and ice-free
314 seasons. For this purpose, we employed the new Bayesian calibration for the mean temperature

315 of the Months Above Freezing (MAF), as proposed by Martínez-Sosa et al. (2021), to derive a
316 MAF for Gahai lake.

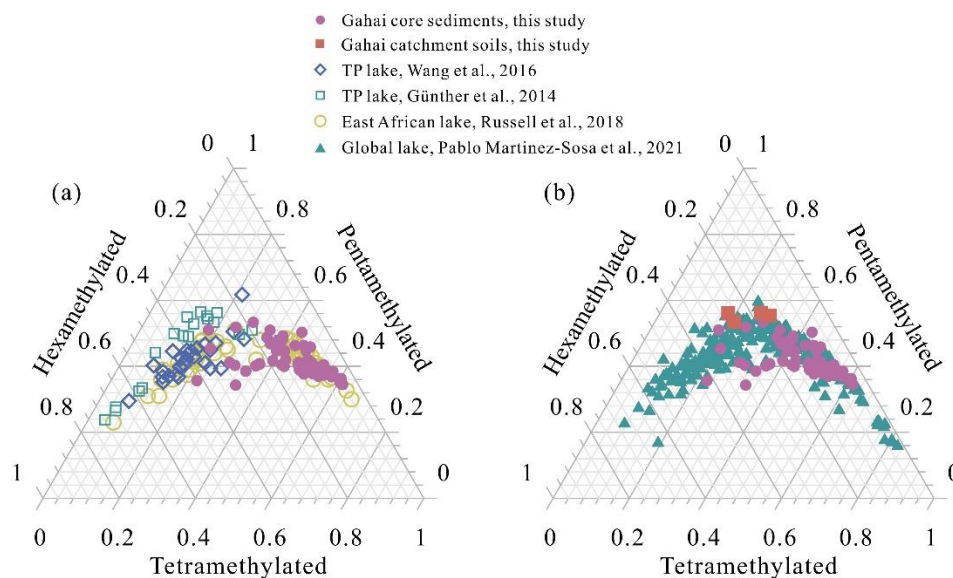
317

318 To assess the accuracy of this calibration approach, we compared the fractional abundances of
319 summed tetra-, penta-, and hexamethylated brGDGTs in Gahai lake sediments with other
320 datasets (Fig. 4). These datasets include lake sediments from the TP (Günther et al., 2014; Wang
321 et al., 2016), East Africa (Russell et al., 2018), and global lakes (Martínez-Sosa et al., 2021).
322 The distribution pattern of Gahai core sediments is distinctly remarkable compared to that of
323 other lake sediments within the TP, even though they share a common regional origin (Fig. 4).
324 However, its resemblance to the global distribution of brGDGTs in lake sediments is evident.
325 Notably, the calibration developed by Martínez-Sosa et al. (2021) is based on brGDGTs from
326 a global lake dataset.

327

328 Using calibration of Martínez-Sosa's et al. (2021), we reconstructed the surface sediment
329 temperature of Gahai lake, resulting in a temperature estimate of 9.4°C. This reconstructed
330 temperature closely matches the ice-free season temperature recorded by meteorological
331 stations in the Gahai region (8.8°C for May to September). Furthermore, considering the
332 significant contribution of autochthonous brGDGTs in Gahai lake, we also attempted to
333 reconstruct the Holocene paleotemperature record using previously published lake-specific
334 brGDGTs-temperature calibrations (e.g., Günther et al., 2014; Martínez-Sosa et al., 2021;
335 Russell et al., 2018; Sun et al., 2011; Wang et al., 2016). As depicted in Fig. S3, most of these
336 calibrations exhibit qualitatively similar temperature change patterns when applied to the

337 sediment core from Gahai lake. This similarity arises from their shared same principles, just
 338 utilizing distinct datasets, resulting in records that display analogous trends but vary in absolute
 339 temperatures.
 340



341
 342 **Fig. 4** Comparison of the fractional abundances of tetramethylated, pentamethylated, and
 343 hexamethylated bGDGTs in sediment core samples from Gahai with lake surface
 344 sediments from the TP (Wang et al., 2016; Günther et al., 2014), East Africa (Russell et
 345 al., 2018), and worldwide (Martínez-Sosa et al., 2021).

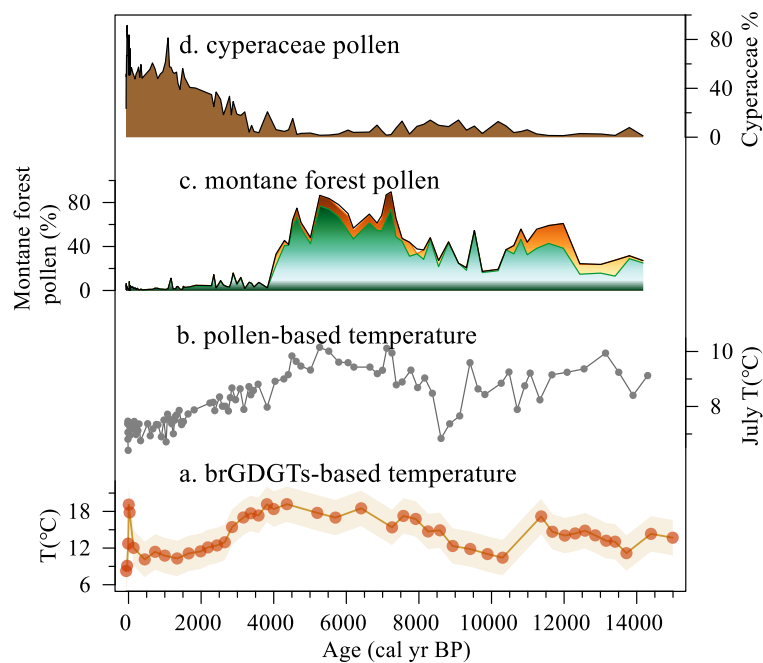
346
 347 The depth interval of 191–279 cm in the Gahai sediment core represents an interval of rapid
 348 allocthonous sedimentation, or alternatively a slump, and therefore the results for the
 349 corresponding time interval of 20–15 ka may be unreliable. Thus, our temperature record of
 350 Months Above Freezing from the eastern TP spans the past 15 ka, with the average temperature
 351 of 4°C, as shown in Fig. 5a. Within the range of age uncertainties, weak warming occurred
 352 during 15–11.8 ka, likely to corresponding to the Bølling–Allerød (B/A) interstadial. A minor
 353 cold reversal occurred during 11.8–10.5 ka, potentially corresponding to the Younger Dryas

354 (YD) event. Notably, the samples collected between 11.8 ka and 10.5 ka exhibited GDGT
355 concentrations below the detection limit. Therefore, we directly linked the temperature
356 reconstructions at the two aforementioned time points, ~11.8 ka and ~10.5 ka, resulting in the
357 lowest temperature of this time period appearing around 10.5 ka. This may cause a time lag
358 with the occurrence of the YD event. The temperature record indicates a colder period during
359 11.5–8.0 ka. During 8.0–3.5 ka, Gahai experienced a stable warm period with the average
360 temperature of ~16.5°C, after which the temperature decreased gradually. Overall, the
361 maximum temperature difference since 15 ka was ~10°C. As for the absolute temperature
362 changes since 15,000 yr, although some influential studies indicate a warming of
363 approximately 6.1-7°C from the deglaciation onset to preindustrial times (Tierney et al., 2020;
364 Osman et al., 2021). However, these results are based on global mean sea surface temperatures.
365 Our reconstructed temperature range is about 10°C, considering the remarkable ‘elevation-
366 dependent warming’ observed in high-altitude regions compared to low-altitude areas
367 (Mountain Initiative EDW Working Group, 2015). Thus, this range could be accurate.
368 Nevertheless, we do not rule out the possibility that our temperature reconstruction may exhibit
369 an overestimation. Aside from potential uncertainties associated with the biomarkers
370 themselves, calibrations may also considerably influence the observed amplitude. We
371 examined temperature variations reconstructed using different calibrations (Fig. S3), with the
372 smallest range being 6°C and the largest being 12°C. Undoubtedly, further efforts are needed
373 to constrain the inherent uncertainties related to biomarker-based temperature reconstructions.

374

375 *3.4 Holocene temperature changes on the eastern edge of TP and their origin*

376 Despite the difference in amplitude, the temperature record of MAF from Gahai resembles the
 377 pollen record and the pollen-based temperature reconstruction from the same site (Fig. 5)
 378 (Wang et al., 2022). However, the brGDGTs-based Holocene Thermal Maximum (HTM) lags
 379 the pollen-based reconstruction (Fig. 5a, b). Wang et al. (2022) used a weighted-averaging
 380 partial least regression approach to produce a temperature record for Gahai, based on a modern
 381 pollen dataset (n=731) from the eastern TP. Assessment of the statistical significance of the
 382 pollen-based climate variables for Gahai suggests that the mean July temperature is the most
 383 important environmental factor influencing the fossil pollen assemblages. The brGDGTs in
 384 Gahai are indicative of summer and autumn temperatures, and the mismatch between the
 385 temperature records inferred from brGDGTs and the pollen record may be attributed to the
 386 difference between the solar irradiance during June–October and that during July. A detailed
 387 analysis of this topic will be undertaken in the subsequent section.

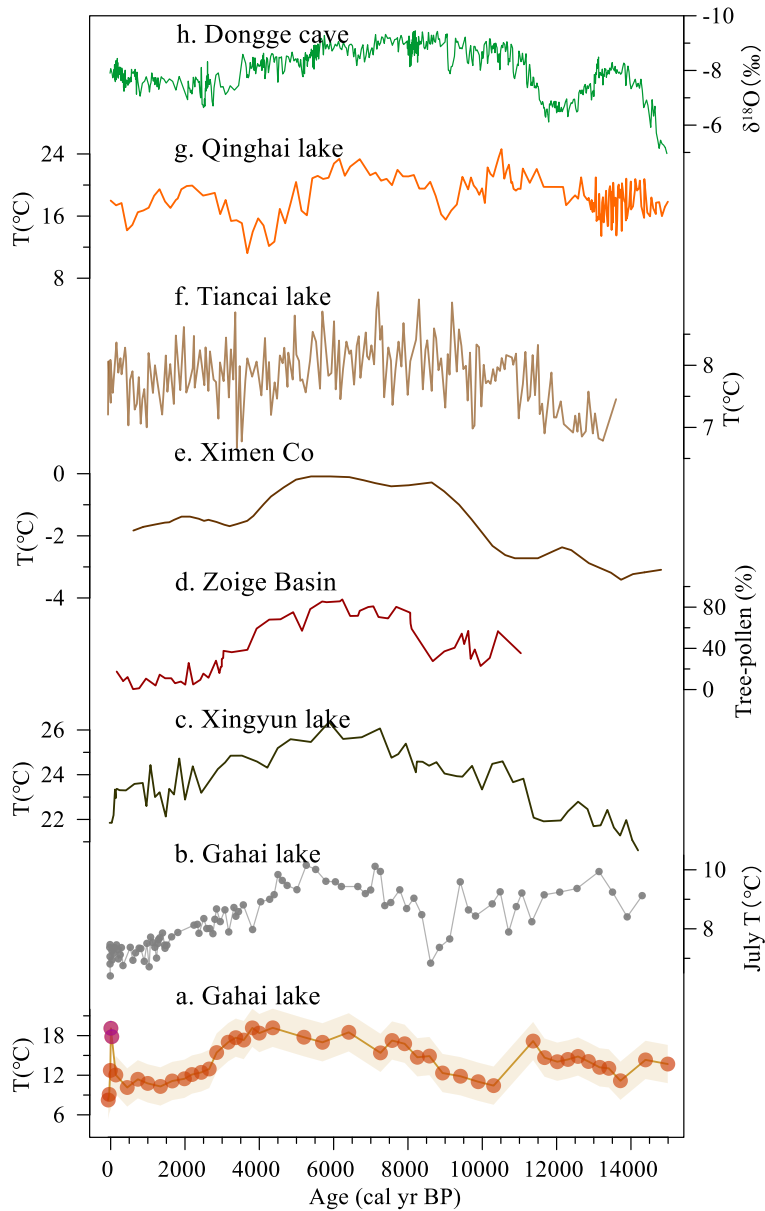


388
 389 **Fig. 5** Comparison of multiproxy records from Gahai lake. (a) brGDGTs-based MAF (this
 390 study). (b) Temperature of the warmest month (July) based on pollen assemblages

391 (Wang et al., 2022). (c, d) Pollen-reconstructed montane forest (*Pinus*, *Picea*, *Abies*) and
392 Cyperaceae pollen record (Wang et al., 2022).

393

394 The brGDGTs-based temperature record from Gahai confirms the occurrence of a climate
395 optimum in the mid-Holocene on the northeast TP, which is consistent with several other pollen
396 and pollen-reconstructed temperature records from the fringe areas of the Asian summer
397 monsoon (Fig. 6), suggesting that it is a reliable representation of Holocene temperature
398 changes in this region. For example, pollen-based temperature reconstructions from Xingyun
399 lake and Ximen Co on the eastern TP show an early to middle HTM (9–4 ka) and a cooling
400 trend thereafter (Fig. 6c, e) (Wu et al., 2018; Herzschuh et al., 2014; Wang et al., 2021a).
401 Additionally, lake water temperature reconstructions based on subfossil chironomids from
402 Tiancai lake (Fig. 6f) (Zhang et al., 2017; Zhang et al., 2019a) and alkenones from Qinghai
403 lake (Fig. 6g) (Hou et al., 2016) show the same trends during the past 15 ka, as also shown by
404 other pollen-based temperature records from the TP (Chen et al., 2020). Pollen, chironomids
405 and alkenones mainly respond to the growing season temperatures in middle and high latitudes,
406 and thus the reconstructed temperature records are consistent with the variations in summer
407 solar irradiance. Similar variations were documented in temperature reconstructions at a global
408 scale (Marcott et al., 2013; Cartapanis et al., 2022). Nevertheless, the timing and amplitude of
409 the Gahai temperature fluctuations differ from those of other temperature records from this
410 region (Fig. 6). These discrepancies may be the result of the chronological uncertainties of
411 these records, and related to differences in the seasonal and spatial responses to climate forcing
412 and feedbacks.



413

414 **Fig. 6** Comparison of temperature at Gahai and other records from the eastern edge of the TP.

415 (a) brGDGTs-based MAF at Gahai, the purple dots may indicate unreliable temperature

416 changes influenced by human activities (this study). (b) Temperature of the warmest

417 month (July) based on pollen data from Gahai (Wang et al., 2022). (c) Pollen-based

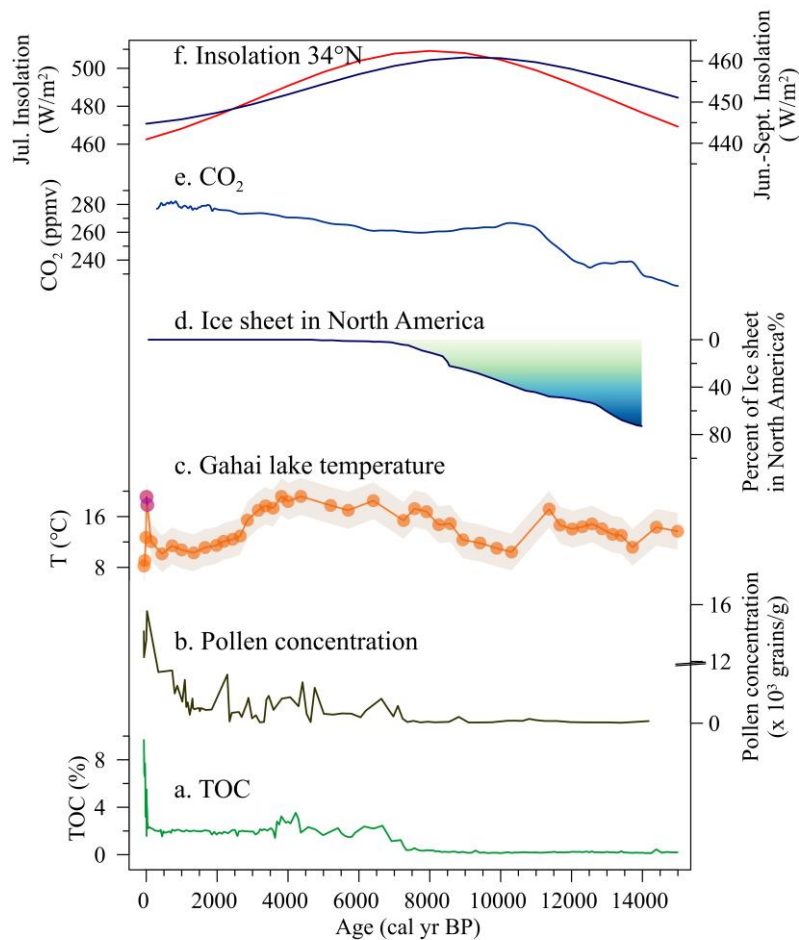
418 temperature at Xingyun lake (Wu et al., 2018). (d) Tree pollen percentages from the

419 Hongyuan peatland in the southern Zoige Basin (Zhou et al., 2010). (e) Pollen-based

420 temperature at Ximen Co (Herzschuh et al., 2014). (f) Chironomid-based temperature at

421 Tiancai lake (Zhang et al., 2017, 2019a). (g) Alkenone-based temperature at Qinghai

422 lake (Hou et al., 2016). (h) Stalagmite $\delta^{18}\text{O}$ record of Dongge cave (Dykoski et al., 2005).



424

425 **Fig. 7** Temperature fluctuations and forcing factors during the Holocene. (a, b) TOC content
 426 and pollen concentrations from Gahai (Wang et al., 2022). (c) brGDGTs-based MAF
 427 from Gahai, the purple dots may indicate unreliable temperature changes influenced by
 428 human activities (this study). (d) Percentage of the remnant Laurentide ice sheet in
 429 North America relative to the Last Glacial Maximum (Dyke, 2004). (e) Variation of
 430 atmospheric CO₂ content (Monnin et al., 2004). (f) Mean insolation during July (W/m²)
 431 (navy blue curve) and mean insolation during ice-free months (W/m²) at 34 °N (red
 432 curve) (Berger and Loutre, 1991; Berger et al., 2010).

433

434 The temperature record in Gahai during the early Holocene fails to closely track the Northern
435 Hemisphere insolation trend, and there is also a time lag. The pollen-based temperature record
436 for Xingyun Lake in southwestern China also shows lower temperatures in the early Holocene
437 (Fig. 6c). The albedo effect caused by the increased cloud cover may be the reason for the early
438 Holocene decrease in summer temperatures (Wu et al., 2018). However, the pollen record from
439 Gahai indicates dry conditions during the early Holocene (Wang et al., 2022), and cloud cover
440 may not be the primary factor responsible for the low temperatures at this time. The melting of
441 Northern Hemisphere ice sheets during the early Holocene would weaken the Atlantic
442 Meridional Overturning Circulation (AMOC) and potentially also the global thermohaline
443 circulation. This would lead to a reduction in the amount of heat transport by the North Atlantic
444 warm current to high-latitude regions and a cooling in middle to high latitudes of the Northern
445 Hemisphere. The persistence of the Laurentide ice sheet into the early Holocene maintained
446 the regional albedo, as well as discharging meltwater into the North Atlantic (Fig. 7d) (Dyke,
447 2004). Furthermore, the cooling during the early Holocene followed by the warming trend in
448 the mid-Holocene potentially correlates with significant fluctuations in CO₂ concentrations
449 within these intervals (Fig. 7e) (Monnin et al., 2004). In addition, a Holocene temperature
450 simulation showed that global warming was more pronounced when dust factors were excluded
451 from the simulation (Liu et al. (2018). The record of insoluble particles in the Greenland GISP2
452 ice core indicates relatively high concentrations of atmospheric aerosols in the early Holocene
453 (Zielinski and Mershon, 1997), which would have weakened summer solar irradiation via
454 radiative feedback, leading to the cool temperatures during this period. In essence, temperature,
455 especially seasonal variations like the Gahai ice-free temperature in the eastern TP, is

456 influenced by multifaceted factors including astronomical forcing, CO₂, and ice sheets.
457 Temperature exhibits varied sensitivities in response to these factors, while both insolation and
458 CO₂ exert considerable and favorable impacts on summer temperature patterns (Lyu and Yin,
459 2022). These factors may together have caused the early Holocene temperature decline at Gahai
460 lake, which slightly delayed the onset of the Holocene Warm Period.

461

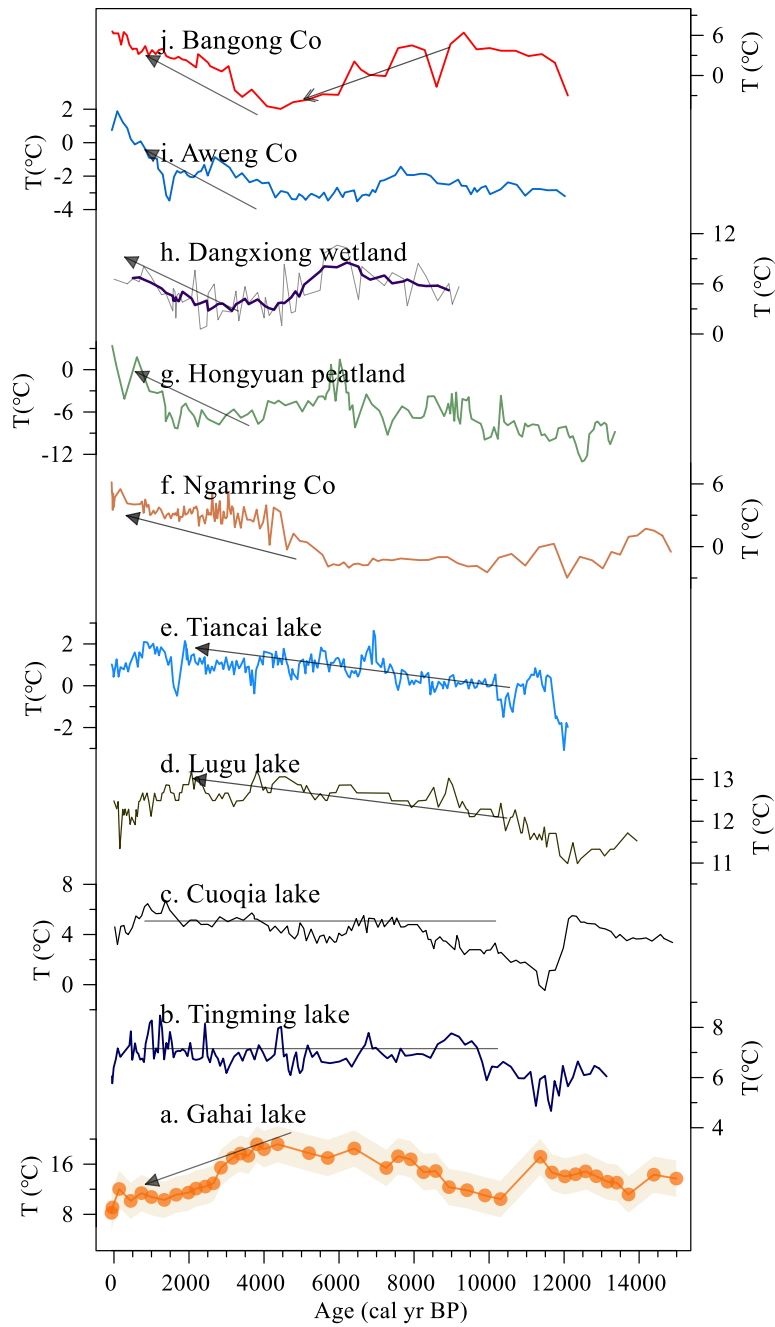
462 A notable and rapid temperature increase is evident at Gahai in recent decades, which differs
463 from the other records (Fig. 7c). Moreover, there are notable increases in pollen concentration,
464 TOC, and TN (Fig. 7a, b) in the Gahai sediment core, indicating intensive local human activities
465 like grazing and tourism, which may be the primary cause of the environmental changes in this
466 region (Wang et al., 2022). This intensive human activity may have reduced the ability of the
467 brGDGTs to record the natural temperature background. These observations emphasize the
468 important impact of human activities on climate proxies and the need to carefully consider their
469 effect on temperature reconstructions.

470

471 *3.5 Spatiotemporal pattern of brGDGTs-based TP temperatures*

472 In addition to comparing the Gahai temperature with the summer temperature records from the
473 eastern TP and its surrounding areas, we compiled and reviewed published Holocene
474 brGDGTs-based quantitative temperature records from across the TP. As shown in Fig. 8, with
475 the increasing number of these records for the TP, the differences between the results have
476 become more pronounced. The brGDGTs records from lakes in the central and western parts
477 of the plateau show higher temperatures in the early and late Holocene, and lower temperatures

478 in the middle Holocene (Wang et al., 2021c; Li et al., 2017; He et al., 2020), while the brGDGTs
479 records from lakes in the southern and south-eastern parts of the TP show a warming trend
480 throughout the Holocene (Sun et al., 2022; Feng et al., 2022). In addition, brGDGTs in Cuoqia
481 lake and Tingming lake, on the south-eastern TP, recorded the ice-free season temperature,
482 which was relatively stable during the Holocene (Sun et al., 2021; Zhang et al., 2022a).
483 However, our temperature record from Gahai is different from the above records and resembles
484 summer temperature changes during the Holocene (Chen et al., 2020). This is because the
485 brGDGTs record from Gahai lake represents warm season temperatures, which adds to its
486 reliability.



487

488 **Fig. 8** Comparison of Holocene temperature based on brGDGTs at Gahai (a) and other

489 records from around the TP. Reconstructed ice-free-season temperatures from (b)

490 Tingming lake (Sun et al., 2021), (c) Cuoqia lake (Zhang et al., 2022a). Reconstructed

491 annual temperature from (d) Lugu lake (Zhao et al., 2021b), (e) Tiancai lake (Feng et al.,

492 2022), (f) Ngamring Co (Sun et al., 2022), (g) Hongyuan peatland (Yan et al., 2021). (h)

493 Dangxiong wetland (Cheung et al., 2017), (i) Aweng Co (Li et al., 2017), (j) Bangong

494 Co (Wang et al., 2021c).

495

496 We suggest that the complexity of Holocene temperature patterns recorded by brGDGTs in TP
497 lakes is primarily due to the ambiguity of brGDGTs in these lakes, as well as to the spatial
498 heterogeneity of climate change across the TP. This ambiguity can be attributed to several
499 factors. First, the origin of brGDGTs in lakes remains an uncertain factor in temperature
500 reconstruction. An increasing number of studies indicate the occurrence of a remarkable
501 amount of autochthonous brGDGTs in lakes, but their abundance in soil can also affect the
502 distribution of brGDGTs in lakes due to their supply via soil erosion (e.g., Tierney and Russell,
503 2009; Weber et al., 2015; Wang et al., 2023). In fact, even within the same lake (e.g.,
504 Tengchongqinghai lake in southwestern China), two studies reached inconsistent conclusions
505 regarding the origin of brGDGTs (Tian et al., 2019; Zhao et al., 2021b), possibly because the
506 niches of certain brGDGTs may expand or contract compared to other locations within a lake.
507 Therefore, it is important to conduct detailed modern process studies to accurately assess the
508 sources of brGDGTs in lakes, especially with regard to evaluating the proportion of
509 autochthonous brGDGTs (Wang et al., 2023; Martin et al., 2020). Second, brGDGTs may show
510 a seasonal signal. Current brGDGTs–temperature calibrations for lakes reflect the annual
511 average temperature (Sun et al., 2011; De Jonge et al., 2014), as well as the growing season
512 temperature (Sun et al., 2011; Dang et al., 2018) and the ice-free season temperature (Martínez-
513 Sosa et al., 2021; Zhang et al., 2022a). Thus, there is no consensus regarding whether the
514 brGDGTs have a seasonal bias, and it is necessary to conduct continuous, high-resolution
515 seasonal investigations of lakes on the TP to comprehensively elucidate the seasonal

516 characteristics of brGDGTs. This can enhance the accuracy of regional temperature
517 reconstruction and may help reconcile the complex temperature patterns observed on the TP.
518 Third, the factors affecting the distribution of brGDGTs in lakes are complex, including not
519 only temperature, pH and salinity but also oxygen content, water depth, and so on (Wang et al.,
520 2021b; Wang et al., 2016). The distribution of brGDGTs in lakes is significantly influenced by
521 the hydrological and physical properties of the lakes, and thus it is necessary to attain a more
522 comprehensive understanding of the characteristics of the lakes in the study area and their
523 effects on brGDGTs. Fourth, different brGDGTs–temperature calibrations may lead to
524 markable differences in both the amplitude and trend of temperature from the same dataset
525 (Wang et al., 2016; Feng et al., 2019). One reason for this is the deviation between in-situ
526 measured temperature and atmospheric temperature (Wang et al., 2020). Thus, selecting an
527 appropriate calibration and attempting to establish a brGDGTs-in situ temperature calibration
528 are effective means of enhancing the reliability of brGDGTs-based temperature reconstructions.

529

530 **4 Conclusions**

531 We present a quantitative, brGDGTs-based seasonal paleotemperature record over the last 15
532 ka from the sediments of a shallow lake on the eastern TP. Our reconstruction resembles the
533 summer temperature trend, with the Holocene Thermal Maximum occurring during 8–3.5 ka.
534 There is a lag between our brGDGTs-based reconstruction and pollen-based temperature
535 recorded in the same sediment core, indicating a seasonal bias between different proxies. Since
536 3.5 ka, the temperature decreased gradually, and the surficial sediments reliably recorded the
537 warm season temperature during the current period in the Gahai lake region. However,

538 intensive local human activity during the last century has affected the distribution of brGDGTs,
539 resulting in temperature deviations recorded by brGDGTs. However, the implementation of
540 environmental protection policies have reduced this anthropogenic signal. Our findings help
541 better understand the seasonal signal of brGDGTs in shallow lakes and provide important data
542 for improving projections of terrestrial climate change at high elevations.

543

544 We also investigated previously published brGDGTs-based Holocene temperature records on
545 the TP to determine the pattern of brGDGTs-based temperature changes and the possible causes
546 of the differences between reconstructions. We emphasize the need for the careful examination
547 of both the source and behavior of these compounds in lacustrine environments and lake status,
548 prior to the application of brGDGTs proxies in paleolimnological reconstruction.

549

550 **Data availability**

551 The data used in this study can be obtained from the corresponding author Juzhi Hou
552 (houjz@itpcas.ac.cn).

553

554 **Author contributions**

555 Xiaohuan Hou did the experiments, analyzed the data and wrote the manuscript. Nannan Wang,
556 Zhe Sun, Kan Yuan and Xianyong Cao participated in sample collecting and data analysis.
557 Juzhi Hou designed this study and led the interpretation. All authors commented on and
558 improved the manuscript.

559

560 **Competing interests**

561 The contact author has declared that none of the authors has any competing interests.

562

563 **Acknowledgements**

564 This work was financially supported by the National Natural Science Foundation of China

565 (42025103, 41877459) and the Second Tibetan Plateau Scientific Expedition and Research

566 (2019QZKK0601). We are grateful to two anonymous reviewers and handling editor Dr.

567 Qiuzhen Yin for their valuable comments which significantly improved the quality of the

568 manuscript. We would like to thank Jan Bloemendal for the help with language editing.

569

570 **References**

571

572 Berger, A. and Loutre, M. F.: Insolation values for the climate of the last 10000000 years, *Quaternary Sci. Rev.*,
573 10, 297-317, 10.1016/0277-3791(91)90033-q, 1991.

574 Berger, A., Loutre, M. F., and Yin, Q. Z.: Total irradiation during any time interval of the year using elliptic
575 integrals, *Quaternary Sci. Rev.*, 29, 1968-1982, 10.1016/j.quascirev.2010.05.007, 2010.

576 Bova, S., Rosenthal, Y., Liu, Z., Godad, S. P., and Yan, M.: Seasonal origin of the thermal maxima at the Holocene
577 and the last interglacial, *Nature*, 589, 548-553, 10.1038/s41586-020-03155-x, 2021.

578 Buckles, L. K., Weijers, J. W. H., Verschuren, D., and Damste, J. S. S.: Sources of core and intact branched
579 tetraether membrane lipids in the lacustrine environment: Anatomy of Lake Challa and its catchment,
580 equatorial East Africa, *Geochim. Cosmochim. Acta.*, 140, 106-126, 10.1016/j.gca.2014.04.042, 2014.

581 Cao, J., Rao, Z., Shi, F., and Jia, G.: Ice formation on lake surfaces in winter causes warm-season bias of lacustrine
582 brGDGT temperature estimates, *Biogeosciences*, 17, 2521-2536, 10.5194/bg-17-2521-2020, 2020.

583 Cartapanis, O., Jonkers, L., Moffa-Sanchez, P., Jaccard, S. L., and de Vernal, A.: Complex spatio-temporal
584 structure of the Holocene Thermal Maximum, *Nat. Commun.*, 13, 5662, 10.1038/s41467-022-33362-1, 2022.

585 Chen, D., Xu, B., Yao, T., Guo, Z., Cui, P., Chen, F., Zhang, R., Zhang, X., Zhang, Y., Fan, J., Hou, Z., and Zhang,
586 T.: Assessment of past, present and future environmental changes on the Tibetan Plateau, *Chinese Sci. Bull.*,
587 60, 3025-3035, 2015.

588 Chen, F., Yu, Z., Yang, M., Ito, E., Wang, S., Madsen, D. B., Huang, X., Zhao, Y., Sato, T., Birks, H. J. B.,
589 Boomer, I., Chen, J., An, C., and Wünnemann, B.: Holocene moisture evolution in arid central Asia and
590 its out-of-phase relationship with Asian monsoon history, *Quaternary Sci. Rev.*, 27, 351-364,
591 10.1016/j.quascirev.2007.10.017, 2008.

592 Chen, F., Zhang, J., Liu, J., Cao, X., Hou, J., Zhu, L., Xu, X., Liu, X., Wang, M., Wu, D., Huang, L., Zeng,
593 T., Zhang, S., Huang, W., Zhang, X., and Yang, K.: Climate change, vegetation history, and landscape
594 responses on the Tibetan Plateau during the Holocene: A comprehensive review, *Quaternary Sci. Rev.*,
595 243, 10.1016/j.quascirev.2020.106444, 2020.

596 Chen, Y., Zheng, F., Yang, H., Yang, W., Wu, R., Liu, X., Liang, H., Chen, H., Pei, H., Zhang, C., Pancost,
597 R. D., and Zeng, Z.: The production of diverse brGDGTs by an Acidobacterium providing a
598 physiological basis for paleoclimate proxies, *Geochim. Cosmochim. Acta.*, 337, 155-165,
599 10.1016/j.gca.2022.08.033, 2022.

600 Cheung, M.-C., Zong, Y., Zheng, Z., Liu, Z., and Aitchison, J. C.: Holocene temperature and precipitation
601 variability on the central Tibetan Plateau revealed by multiple palaeo-climatic proxy records from an alpine
602 wetland sequence, *The Holocene*, 27, 1669-1681, 10.1177/0959683617702225, 2017.

603 Crampton-Flood, E. D., Tierney, J. E., Peterse, F., Kirkels, F. M. S. A., and Damste, J. S. S.: BayMBT: A Bayesian
604 calibration model for branched glycerol dialkyl glycerol tetraethers in soils and peats, *Geochim. Cosmochim.*
605 *Acta.*, 268, 142-159, 10.1016/j.gca.2019.09.043, 2020.

606 Dang, X., Ding, W., Yang, H., Pancost, R. D., Naafs, B. D. A., Xue, J., Lin, X., Lu, J., and Xie, S.: Different
607 temperature dependence of the bacterial brGDGT isomers in 35 Chinese lake sediments compared to that in
608 soils, *Org. Geochem.*, 119, 72-79, 10.1016/j.orggeochem.2018.02.008, 2018.

609 De Jonge, C., Hopmans, E. C., Zell, C. I., Kim, J.-H., Schouten, S., and Sinninghe Damsté, J. S.: Occurrence and
610 abundance of 6-methyl branched glycerol dialkyl glycerol tetraethers in soils: Implications for palaeoclimate
611 reconstruction, *Geochim. Cosmochim. Acta.*, 141, 97-112, 10.1016/j.gca.2014.06.013, 2014.

612 Ding, S., Xu, Y., Wang, Y., He, Y., Hou, J., Chen, L., and He, J. S.: Distribution of branched glycerol dialkyl
613 glycerol tetraethers in surface soils of the Qinghai-Tibetan Plateau: implications of brGDGTs-based proxies

614 in cold and dry regions, *Biogeosciences*, 12, 3141-3151, 10.5194/bg-12-3141-2015, 2015.

615 Dong, Y., Wu, N., Li, F., Zhang, D., Zhang, Y., Shen, C., and Lu, H.: The Holocene temperature conundrum
616 answered by mollusk records from East Asia, *Nat. Commun.*, 13, 5153, 10.1038/s41467-022-32506-7, 2022.

617 Dyke, A. S.: An outline of North American deglaciation with emphasis on central and northern Canada,
618 Quaternary Glaciations-Extent and Chronology, Pt 2: North America, 2, 373-424, 10.1016/s1571-
619 0866(04)80209-4, 2004.

620 Dykoski, C. A., Edwards, R. L., Cheng, H., Yuan, D. X., Cai, Y. J., Zhang, M. L., Lin, Y. S., Qing, J. M., An, Z.
621 S., and Revenaugh, J.: A high-resolution, absolute-dated Holocene and deglacial Asian monsoon record from
622 Dongge Cave, China, *Earth Planet. Sc. Lett.*, 233, 71-86, 10.1016/j.epsl.2005.01.036, 2005.

623 Feng, X., Zhao, C., D'Andrea, W. J., Liang, J., Zhou, A., and Shen, J.: Temperature fluctuations during the
624 Common Era in subtropical southwestern China inferred from brGDGTs in a remote alpine lake, *Earth Planet.
625 Sc. Lett.*, 510, 26-36, 10.1016/j.epsl.2018.12.028, 2019.

626 Feng, X., Zhao, C., D'Andrea, W. J., Hou, J., Yang, X., Xiao, X., Shen, J., Duan, Y., and Chen, F.: Evidence for a
627 Relatively Warm Mid-to Late Holocene on the Southeastern Tibetan Plateau, *Geophys. Res. Lett.*, 49,
628 10.1029/2022gl098740, 2022.

629 Group, M. I. E. W.: Elevation-dependent warming in mountain regions of the world, *Nat. Clim. Change*, 5, 424-
630 430, 10.1038/nclimate2563, 2015.

631 Günther, F., Thiele, A., Gleixner, G., Xu, B., Yao, T., and Schouten, S.: Distribution of bacterial and archaeal ether
632 lipids in soils and surface sediments of Tibetan lakes: Implications for GDGT-based proxies in saline high
633 mountain lakes, *Org. Geochem.*, 67, 19-30, 10.1016/j.orggeochem.2013.11.014, 2014.

634 Halamka, T. A., Raberg, J. H., McFarlin, J. M., Younkin, A. D., Mulligan, C., Liu, X. L., and Kopf, S. H.:
635 Production of diverse brGDGTs by *Acidobacterium Solibacter usitatus* in response to temperature, pH, and
636 O₂ provides a culturing perspective on brGDGT proxies and biosynthesis, *Geobiology*, 10.1111/gbi.12525,
637 2022.

638 He, Y., Hou, J., Wang, M., Li, X., Liang, J., Xie, S., and Jin, Y.: Temperature Variation on the Central Tibetan
639 Plateau Revealed by Glycerol Dialkyl Glycerol Tetraethers From the Sediment Record of Lake Linggo Co
640 Since the Last Deglaciation, *Front. Earth Sci.*, 8, 10.3389/feart.2020.574206, 2020.

641 Herzschuh, U., Borkowski, J., Schewe, J., Mischke, S., and Tian, F.: Moisture-advection feedback supports strong
642 early-to-mid Holocene monsoon climate on the eastern Tibetan Plateau as inferred from a pollen-based
643 reconstruction, *Paleogeogr. Paleocl.*, 402, 44-54, 10.1016/j.palaeo.2014.02.022, 2014.

644 Hou, J., Li, C., and Lee, S.: The temperature record of the Holocene: progress and controversies, *Sci. Bull.*,
645 10.1016/j.scib.2019.02.012, 2019.

646 Hou, J., Huang, Y., Zhao, J., Liu, Z., Colman, S., and An, Z.: Large Holocene summer temperature oscillations
647 and impact on the peopling of the northeastern Tibetan Plateau, *Geophys. Res. Lett.*, 43, 1323-1330,
648 10.1002/2015gl067317, 2016.

649 Huguet, C., Hopmans, E. C., Febo-Ayala, W., Thompson, D. H., Sinninghe Damsté, J. S., and Schouten, S.: An
650 improved method to determine the absolute abundance of glycerol dibiphytanyl glycerol tetraether lipids,
651 *Org. Geochem.*, 37, 1036-1041, 10.1016/j.orggeochem.2006.05.008, 2006.

652 Kuang, X. and Jiao, J. J.: Review on climate change on the Tibetan Plateau during the last half century, *J. Geophys.
653 Res.-Atmos.*, 121, 3979-4007, 10.1002/2015jd024728, 2016.

654 Li, X., Wang, M., Zhang, Y., Lei, L., and Hou, J.: Holocene climatic and environmental change on the western
655 Tibetan Plateau revealed by glycerol dialkyl glycerol tetraethers and leaf wax deuterium-to-hydrogen ratios
656 at Aweng Co, *Quat Res.*, 87, 455-467, 10.1017/qua.2017.9, 2017.

657 Liang, W. and Luo, A.: *Luqu County Annals*, Gansu Culture Press, Lanzhou, 71 pp.2006 (in Chinese).

658 Liu, Y., Zhang, M., Liu, Z., Xia, Y., Huang, Y., Peng, Y., and Zhu, J.: A Possible Role of Dust in Resolving the
659 Holocene Temperature Conundrum, *Sci. Rep.*, 8, 10.1038/s41598-018-22841-5, 2018.

660 Liu, Z. Y., Zhu, J., Rosenthal, Y., Zhang, X., Otto-Bliesner, B. L., Timmermann, A., Smith, R. S., Lohmann, G.,
661 Zheng, W. P., and Timm, O. E.: The Holocene temperature conundrum, *Proc. Natl. Acad. Sci. USA.*, 111,
662 E3501-E3505, 10.1073/pnas.1407229111, 2014.

663 Loomis, S. E., Russell, J. M., Heureux, A. M., D'Andrea, W. J., and Sinninghe Damsté, J. S.: Seasonal variability
664 of branched glycerol dialkyl glycerol tetraethers (brGDGTs) in a temperate lake system, *Geochim.*
665 *Cosmochim. Acta.*, 144, 173-187, 10.1016/j.gca.2014.08.027, 2014.

666 Lu, H., Wu, N., Liu, K.-b., Zhu, L., Yang, X., Yao, T., Wang, L., Li, Q., Liu, X., Shen, C., Li, X., Tong, G., and
667 Jiang, H.: Modern pollen distributions in Qinghai-Tibetan Plateau and the development of transfer functions
668 for reconstructing Holocene environmental changes, *Quaternary Sci. Rev.*, 30, 947-966,
669 10.1016/j.quascirev.2011.01.008, 2011.

670 Lyu, A. and Yin, Q. Z.: The spatial-temporal patterns of East Asian climate in response to insolation, CO₂ and ice
671 sheets during MIS-5, *Quaternary Sci. Rev.*, 293, 10.1016/j.quascirev.2022.107689, 2022.

672 Ma, W., Li, G., Song, J., Yan, L., and Wu, L.: Effect of Vegetation Degradation on Soil Organic Carbon Pool and
673 Carbon Pool Management Index in the Gahai Wetland, China, *Acta Agrestia Sinica*, 27, 687-694, 2019.

674 Marcott, S. A., Shakun, J. D., Clark, P. U., and Mix, A. C.: A Reconstruction of Regional and Global Temperature
675 for the Past 11,300 Years, *Science*, 339, 1198-1201, 10.1126/science.1228026, 2013.

676 Marsicek, J., Shuman, B. N., Bartlein, P. J., Shafer, S. L., and Brewer, S.: Reconciling divergent trends and
677 millennial variations in Holocene temperatures, *Nature*, 554, 92+, 10.1038/nature25464, 2018.

678 Martin, C., Ménot, G., Thouveny, N., Peyron, O., Andrieu-Ponel, V., Montade, V., Davtian, N., Reille, M., and
679 Bard, E.: Early Holocene Thermal Maximum recorded by branched tetraethers and pollen in Western Europe
680 (Massif Central, France), *Quaternary Sci. Rev.*, 228, 106109, 10.1016/j.quascirev.2019.106109, 2020.

681 Martínez-Sosa, P., Tierney, J. E., Stefanescu, I. C., Dearing Crampton-Flood, E., Shuman, B. N., and Routsom, C.:
682 A global Bayesian temperature calibration for lacustrine brGDGTs, *Geochim. Cosmochim. Acta.*, 305, 87-
683 105, 10.1016/j.gca.2021.04.038, 2021.

684 Monnin, E., Steig, E. J., Siegenthaler, U., Kawamura, K., Schwander, J., Stauffer, B., Stocker, T. F., Morse, D. L.,
685 Barnola, J. M., Bellier, B., Raynaud, D., and Fischer, H.: Evidence for substantial accumulation rate
686 variability in Antarctica during the Holocene, through synchronization of CO₂ in the Taylor Dome, Dome C
687 and DML ice cores, *Earth Planet. Sc. Lett.*, 224, 45-54, 10.1016/j.epsl.2004.05.007, 2004.

688 Moser, K. A., Baron, J. S., Brahney, J., Oleksy, I. A., Saros, J. E., Hundey, E. J., Sadro, S., Kopáček, J., Sommaruga,
689 R., Kainz, M. J., Strecker, A. L., Chandra, S., Walters, D. M., Preston, D. L., Michelutti, N., Lepori, F.,
690 Spaulding, S. A., Christianson, K. R., Melack, J. M., and Smol, J. P.: Mountain lakes: Eyes on global
691 environmental change, *Glob. Planet Change*, 178, 77-95, 10.1016/j.gloplacha.2019.04.001, 2019.

692 Opitz, S., Zhang, C., Herzsuh, U., and Mischke, S.: Climate variability on the south-eastern Tibetan Plateau
693 since the Lateglacial based on a multiproxy approach from Lake Naleng – comparing pollen and non-pollen
694 signals, *Quaternary Sci. Rev.*, 115, 112-122, 10.1016/j.quascirev.2015.03.011, 2015.

695 Osman, M. B., Tierney, J. E., Zhu, J., Tardif, R., Hakim, G. J., King, J., and Poulsen, C. J.: Globally resolved
696 surface temperatures since the Last Glacial Maximum, *Nature*, 599, 239-244, 10.1038/s41586-021-03984-4,
697 2021.

698 Pang, H., Hou, S., Zhang, W., Wu, S., Jenk, T. M., Schwikowski, M., and Jouzel, J.: Temperature Trends in
699 the Northwestern Tibetan Plateau Constrained by Ice Core Water Isotopes Over the Past 7,000 Years,
700 *J. Geophys. Res.-Atmos.*, 125, 10.1029/2020jd032560, 2020.

701 Qiu, J.: The third pole, *Nature*, 454, 393-396, 10.1038/454393a, 2008.

702 Russell, J. M., Hopmans, E. C., Loomis, S. E., Liang, J., and Sinninghe Damsté, J. S.: Distributions of 5- and 6-
703 methyl branched glycerol dialkyl glycerol tetraethers (brGDGTs) in East African lake sediment: Effects of
704 temperature, pH, and new lacustrine paleotemperature calibrations, *Org. Geochem.*, 117, 56-69,
705 10.1016/j.orggeochem.2017.12.003, 2018.

706 Sinninghe Damsté, J. S., Hopmans, E. C., Pancost, R. D., Schouten, S., and Geenevasen, J. A. J.: Newly discovered
707 non-isoprenoid glycerol dialkyl glycerol tetraether lipids in sediments, *Chem. Commun.*, 1683-1684,
708 10.1039/b004517i, 2000.

709 Sinninghe Damsté, J. S., Ossebaar, J., Abbas, B., Schouten, S., and Verschuren, D.: Fluxes and distribution of
710 tetraether lipids in an equatorial African lake: Constraints on the application of the TEX86
711 palaeothermometer and BIT index in lacustrine settings, *Geochim. Cosmochim. Acta.*, 73, 4232-4249,
712 10.1016/j.gca.2009.04.022, 2009.

713 Sun, Q., Chu, G., Liu, M., Xie, M., Li, S., Ling, Y., Wang, X., Shi, L., Jia, G., and Lü, H.: Distributions and
714 temperature dependence of branched glycerol dialkyl glycerol tetraethers in recent lacustrine sediments from
715 China and Nepal, *J. Geophys. Res.*, 116, 10.1029/2010jg001365, 2011.

716 Sun, X., Zhao, C., Zhang, C., Feng, X., Yan, T., Yang, X., and Shen, J.: Seasonality in Holocene Temperature
717 Reconstructions in Southwestern China, *Paleoceanogr. Paleoicl.*, 36, 10.1029/2020pa004025, 2021.

718 Sun, Z., Hou, X., Ji, K., Yuan, K., Li, C., Wang, M., and Hou, J.: Potential winter-season bias of annual temperature
719 variations in monsoonal Tibetan Plateau since the last deglaciation, *Quaternary Sci. Rev.*, 292,
720 10.1016/j.quascirev.2022.107690, 2022.

721 Thompson, L. G., Yao, T., Davis, M. E., Henderson, K. A., MosleyThompson, E., Lin, P. N., Beer, J., Synal, H.
722 A., ColeDai, J., and Bolzan, J. F.: Tropical climate instability: The last glacial cycle from a Qinghai-Tibetan
723 ice core, *Science*, 276, 1821-1825, 10.1126/science.276.5320.1821, 1997.

724 Tian, L., Wang, M., Zhang, X., Yang, X., Zong, Y., Jia, G., Zheng, Z., and Man, M.: Synchronous change of
725 temperature and moisture over the past 50 ka in subtropical southwest China as indicated by biomarker
726 records in a crater lake, *Quaternary Sci. Rev.*, 212, 121-134, 10.1016/j.quascirev.2019.04.003, 2019.

727 Tierney, J. E. and Russell, J. M.: Distributions of branched GDGTs in a tropical lake system: Implications for
728 lacustrine application of the MBT/CBT paleoproxy, *Org. Geochem.*, 40, 1032-1036,
729 10.1016/j.orggeochem.2009.04.014, 2009.

730 Tierney, J. E., Russell, J. M., Eggermont, H., Hopmans, E. C., Verschuren, D., and Sinninghe Damsté, J. S.:
731 Environmental controls on branched tetraether lipid distributions in tropical East African lake sediments,
732 *Geochim. Cosmochim. Acta.*, 74, 4902-4918, 10.1016/j.gca.2010.06.002, 2010.

733 Tierney, J. E., Zhu, J., King, J., Malevich, S. B., Hakim, G. J., and Poulsen, C. J.: Glacial cooling and climate
734 sensitivity revisited, *Nature*, 584, 569-+, 10.1038/s41586-020-2617-x, 2020.

735 van Bree, L. G. J., Peterse, F., Baxter, A. J., De Crop, W., van Grinsven, S., Villanueva, L., Verschuren, D., and
736 Sinninghe Damsté, J. S.: Seasonal variability and sources of in situ brGDGT production in a permanently
737 stratified African crater lake, *Biogeosciences*, 17, 5443-5463, 10.5194/bg-17-5443-2020, 2020.

738 Wang, G., Wang, Y., Wei, Z., He, W., Ma, X., and Zhang, T.: Reconstruction of temperature and precipitation
739 spanning the past 28 kyr based on branched tetraether lipids from Qionghai Lake, southwestern China,
740 *Paleogeogr. Paleoicl.*, 562, 10.1016/j.palaeo.2020.110094, 2021a.

741 Wang, H., An, Z., Lu, H., Zhao, Z., and Liu, W.: Calibrating bacterial tetraether distributions towards in situ soil
742 temperature and application to a loess-paleosol sequence, *Quaternary Sci. Rev.*, 231,
743 10.1016/j.quascirev.2020.106172, 2020.

744 Wang, H., Chen, W., Zhao, H., Cao, Y., Hu, J., Zhao, Z., Cai, Z., Wu, S., Liu, Z., and Liu, W.: Biomarker-based
745 quantitative constraints on maximal soil-derived brGDGTs in modern lake sediments, *Earth Planet. Sc. Lett.*,

746 602, 10.1016/j.epsl.2022.117947, 2023.

747 Wang, H., Liu, W., He, Y., Zhou, A., Zhao, H., Liu, H., Cao, Y., Hu, J., Meng, B., Jiang, J., Kolpakova, M.,
748 Krivonogov, S., and Liu, Z.: Salinity-controlled isomerization of lacustrine brGDGTs impacts the associated
749 MBT5ME' terrestrial temperature index, *Geochim. Cosmochim. Acta.*, 305, 33-48,
750 10.1016/j.gca.2021.05.004, 2021b.

751 Wang, M., Liang, J., Hou, J., and Hu, L.: Distribution of GDGTs in lake surface sediments on the Tibetan Plateau
752 and its influencing factors, *Sci. China Earth Sci.*, 59, 961-974, 10.1007/s11430-015-5214-3, 2016.

753 Wang, M. D., Hou, J. Z., Duan, Y. W., Chen, J. H., Li, X. M., He, Y., Lee, S. Y., and Chen, F. H.: Internal feedbacks
754 forced Middle Holocene cooling on the Qinghai-Tibetan Plateau, *Boreas*, 10.1111/bor.12531, 2021c.

755 Wang, N., Liu, L., Hou, X., Zhang, Y., Wei, H., and Cao, X.: Palynological evidence reveals an arid early Holocene
756 for the northeast Tibetan Plateau, *Clim. Past.*, 18, 2381-2399, 10.5194/cp-18-2381-2022, 2022.

757 Weber, Y., De Jonge, C., Rijpstra, W. I. C., Hopmans, E. C., Stadnitskaia, A., Schubert, C. J., Lehmann, M. F.,
758 Sinninghe Damsté, J. S., and Niemann, H.: Identification and carbon isotope composition of a novel branched
759 GDGT isomer in lake sediments: Evidence for lacustrine branched GDGT production, *Geochim. Cosmochim.*
760 *Acta.*, 154, 118-129, 10.1016/j.gca.2015.01.032, 2015.

761 Weber, Y., Sinninghe Damsté, J. S., Zopfi, J., De Jonge, C., Gilli, A., Schubert, C. J., Lepori, F., Lehmann, M. F.,
762 and Niemann, H.: Redox-dependent niche differentiation provides evidence for multiple bacterial sources of
763 glycerol tetraether lipids in lakes, *Proc. Natl. Acad. Sci. USA*, 115, 10926-10931, 10.1073/pnas.1805186115,
764 2018.

765 Weijers, J. W. H., Schouten, S., van den Donker, J. C., Hopmans, E. C., and Sinninghe Damsté, J. S.:
766 Environmental controls on bacterial tetraether membrane lipid distribution in soils, *Geochim. Cosmochim.*
767 *Acta.*, 71, 703-713, 10.1016/j.gca.2006.10.003, 2007.

768 Woltering, M., Werne, J. P., Kish, J. L., Hicks, R., Sinninghe Damsté, J. S., and Schouten, S.: Vertical and temporal
769 variability in concentration and distribution of thaumarchaeotal tetraether lipids in Lake Superior and the
770 implications for the application of the TEX86 temperature proxy, *Geochim. Cosmochim. Acta.*, 87, 136-153,
771 10.1016/j.gca.2012.03.024, 2012.

772 Wu, D., Chen, X., Lv, F., Brenner, M., Curtis, J., Zhou, A., Chen, J., Abbott, M., Yu, J., and Chen, F.: Decoupled
773 early Holocene summer temperature and monsoon precipitation in southwest China, *Quaternary Sci. Rev.*,
774 193, 54-67, 10.1016/j.quascirev.2018.05.038, 2018.

775 Wu, J., Yang, H., Pancost, R. D., Naafs, B. D. A., Qian, S., Dang, X., Sun, H., Pei, H., Wang, R., Zhao, S., and
776 Xie, S.: Variations in dissolved O₂ in a Chinese lake drive changes in microbial communities and impact
777 sedimentary GDGT distributions, *Chem. Geol.*, 579, 10.1016/j.chemgeo.2021.120348, 2021.

778 Yan, T., Zhao, C., Yan, H., Shi, G., Sun, X., Zhang, C., Feng, X., and Leng, C.: Elevational differences in Holocene
779 thermal maximum revealed by quantitative temperature reconstructions at ~30° N on eastern Tibetan Plateau,
780 *Paleogeogr. Paleoclimatol.*, 570, 110364, 10.1016/j.palaeo.2021.110364, 2021.

781 Yao, T., Bolch, T., Chen, D., Gao, J., Immerzeel, W., Piao, S., Su, F., Thompson, L., Wada, Y., Wang, L., Wang,
782 T., Wu, G., Xu, B., Yang, W., Zhang, G., and Zhao, P.: The imbalance of the Asian water tower, *Nat. Rev.*
783 *Earth Environ.*, 3, 618-632, 10.1038/s43017-022-00299-4, 2022.

784 Zhang, C., Zhao, C., Yu, S.-Y., Yang, X., Cheng, J., Zhang, X., Xue, B., Shen, J., and Chen, F.: Seasonal imprint
785 of Holocene temperature reconstruction on the Tibetan Plateau, *Earth-Sci. Rev.*, 226, 103927,
786 10.1016/j.earscirev.2022.103927, 2022a.

787 Zhang, E., Chang, J., Shulmeister, J., Langdon, P., Sun, W., Cao, Y., Yang, X., and Shen, J.: Summer temperature
788 fluctuations in Southwestern China during the end of the LGM and the last deglaciation, *Earth Planet. Sc.*
789 *Lett.*, 509, 78-87, 10.1016/j.epsl.2018.12.024, 2019a.

790 Zhang, E., Chang, J., Cao, Y., Sun, W., Shulmeister, J., Tang, H., Langdon, P. G., Yang, X., and Shen, J.: Holocene
791 high-resolution quantitative summer temperature reconstruction based on subfossil chironomids from the
792 southeast margin of the Qinghai-Tibetan Plateau, *Quaternary Sci. Rev.*, 165, 1-12,
793 10.1016/j.quascirev.2017.04.008, 2017.

794 Zhang, G., Luo, W., Chen, W., and Zheng, G.: A robust but variable lake expansion on the Tibetan Plateau, *Sci.*
795 *Bull.*, 64, 1306-1309, 10.1016/j.scib.2019.07.018, 2019b.

796 Zhang, W., Wu, H., Cheng, J., Geng, J., Li, Q., Sun, Y., Yu, Y., Lu, H., and Guo, Z.: Holocene seasonal temperature
797 evolution and spatial variability over the Northern Hemisphere landmass, *Nat. Commun.*, 13, 5334,
798 10.1038/s41467-022-33107-0, 2022b.

799 Zhao, B., Castaneda, I. S., Bradley, R. S., Salacup, J. M., de Wet, G. A., Daniels, W. C., and Schneider, T.:
800 Development of an in situ branched GDGT calibration in Lake 578, southern Greenland, *Org. Geochem.*,
801 152, 10.1016/j.orggeochem.2020.104168, 2021a.

802 Zhao, C., Liu, Z. H., Rohling, E. J., Yu, Z. C., Liu, W. G., He, Y. X., Zhao, Y., and Chen, F. H.: Holocene
803 temperature fluctuations in the northern Tibetan Plateau, *Quat. Res.*, 80, 55-65, 10.1016/j.yqres.2013.05.001,
804 2013.

805 Zhao, C., Rohling, E. J., Liu, Z., Yang, X., Zhang, E., Cheng, J., Liu, Z., An, Z., Yang, X., Feng, X., Sun, X.,
806 Zhang, C., Yan, T., Long, H., Yan, H., Yu, Z., Liu, W., Yu, S.-Y., and Shen, J.: Possible obliquity-forced
807 warmth in southern Asia during the last glacial stage, *Sci. Bull.*, 66, 1136-1145, 10.1016/j.scib.2020.11.016,
808 2021b.

809 Zheng, Y., Li, Q., Wang, Z., Naafs, B. D. A., Yu, X., and Pancost, R. D.: Peatland GDGT records of Holocene
810 climatic and biogeochemical responses to the Asian Monsoon, *Org. Geochem.*, 87, 86-95,
811 10.1016/j.orggeochem.2015.07.012, 2015.

812 Zhou, W., Yu, S.-Y., Burr, G. S., Kukla, G. J., Jull, A. J. T., Xian, F., Xiao, J., Colman, S. M., Yu, H., Liu, Z., and
813 Kong, X.: Postglacial changes in the Asian summer monsoon system: a pollen record from the eastern margin
814 of the Tibetan Plateau, *Boreas*, 39, 528-539, 10.1111/j.1502-3885.2010.00150.x, 2010.

815 Zielinski, G. A. and Mershon, G. R.: Paleoenvironmental implications of the insoluble microparticle record in the
816 GISP2 (Greenland) ice core during the rapidly changing climate of the Pleistocene-Holocene transition, *Geol.*
817 *Soc. Am. Bull.*, 109, 547-559, 10.1130/0016-7606(1997)109<0547:piotim>2.3.co;2, 1997.

818

819